Report

SOURCE DATA | TRANSPARENT PROCESS

EMBO reports

Specific *N*-glycans regulate an extracellular adhesion complex during somatosensory dendrite patterning

Maisha Rahman[1,2], Nelson J Ramirez-Suarez[1,†], Carlos A Diaz-Balzac[1,‡] & Hannes E Bülow[1,2,*]

Abstract

_N_-glycans are molecularly diverse sugars borne by over 70% of proteins transiting the secretory pathway and have been implicated in protein folding, stability, and localization. Mutations in genes important for _N_-glycosylation result in congenital disorders of glycosylation that are often associated with intellectual disability. Here, we show that structurally distinct _N_-glycans regulate an extracellular protein complex involved in the patterning of somatosensory dendrites in _Caenorhabditis elegans_. Specifically, _aman-2/Golgi alpha-mannosidase II_, a conserved key enzyme in the biosynthesis of specific _N_-glycans, regulates the activity of the Menorin adhesion complex without obviously affecting the protein stability and localization of its components. AMAN-2 functions cell-autonomously to allow for decoration of the neuronal transmembrane receptor DMA-1/LRR-TM with the correct set of high-mannose/hybrid/paucimannose _N_-glycans. Moreover, distinct types of _N_-glycans on specific _N_-glycosylation sites regulate DMA-1/LRR-TM receptor function, which, together with three other extracellular proteins, forms the Menorin adhesion complex. In summary, specific _N_-glycan structures regulate dendrite patterning by coordinating the activity of an extracellular adhesion complex, suggesting that the molecular diversity of _N_-glycans can contribute to developmental specificity in the nervous system.

Keywords adhesion; alpha mannosidase II; dendrite; glycosylations; *N*-glycans

Subject Categories Cell Adhesion, Polarity & Cytoskeleton; Neuroscience; Post-translational Modifications & Proteolysis

DOI 10.15252/embr.202154163 | Received 15 October 2021 | Revised 13 April 2022 | Accepted 22 April 2022 | Published online 19 May 2022

EMBO Reports (2022) 23: e54163

Introduction

Development of a nervous system in metazoans requires the coordinated interactions of extracellular molecules to ensure correct neuronal morphogenesis and to establish connectivity (Jan & Jan, 2010; Dong *et al*, 2015; Lefebvre, 2021). Most of these extracellular proteins are glycoconjugates, that is, carry different types of glycans attached to the protein backbone. Glycans are molecularly the most diverse molecules in nature, in part because they are not genetically encoded. Yet their structures are not random and are therefore conceptually attractive to broaden the molecular diversity and specificity of extracellular proteins and their interactions during development. For example, glycosaminoglycans, a class of glycans, have been suggested to modulate protein–protein interactions and provide information during neural development by way of their structural diversity (Holt & Dickson, 2005; Bülow & Hobert, 2006; Poulain & Yost, 2015; Masu, 2016; Saied-Santiago & Bülow, 2018).

N-glycans are another structurally diverse group of glycans that fall into four classes: high-mannose, hybrid, complex, and paucimannose-type *N*-glycans, and are invariantly attached via an asparagine to a protein backbone (Stanley *et al*, 2015). Importantly, 70% of all proteins transiting the endoplasmic reticulum are post-translationally *N*-glycosylated (Apweiler *et al*, 1999). Therefore, the structural diversity of *N*-glycans could also significantly expand the repertoire and specificity of protein interactions or functions in the extracellular space. *N*-glycans in general have been shown to be important for protein folding, stability, localization, and protein–protein interactions (Stanley *et al*, 2015). Moreover, mutations in genes involved in *N*-glycosylation in humans result in congenital disorders of glycosylation (CDG), which are multi-syndromic and often include neurological symptoms, including intellectual disability (Freeze, 2006; Jaeken & Peanne, 2017; Chang *et al*, 2018; Ng & Freeze, 2018). Studies in vertebrates and invertebrates have shown that mutants compromising *N*-glycan biosynthesis or *N*-glycan attachment result in defects in cell surface localization of cell adhesion molecules and axon guidance cues (Sekine *et al*, 2013; Medina-Cano *et al*, 2018; Mire *et al*, 2018). Moreover, *N*-glycosylation *per se* has been shown to be important for dendrite development in dissociated rat neurons (Hanus *et al*, 2016), and the addition of polysialic acid chains to *N*-glycans can change the binding properties of cell adhesion

1 Department of Genetics, Albert Einstein College of Medicine, Bronx, NY, USA
2 Dominick P. Purpura Department of Neuroscience, Albert Einstein College of Medicine, Bronx, NY, USA
*Corresponding author. Tel: +1 718 430 3621; Fax: +1 718 430 8778; E-mail: hannes.buelow@einsteinmed.edu
†Present address: Institute of Science and Technology Austria, Klosterneuburg, Austria
‡Present address: University of Rochester, Rochester, NY, USA

molecules (reviewed in Schnaar *et al*, 2014). However, the question of whether and how specific classes and structures of *N*-glycans modulate extracellular pathways or complexes during nervous system development *in vivo* remains understudied.

Here we use the dendrites of the somatosensory PVD neuron (Posterior cell body, Ventral cord process D), which display complex and stereotyped branching patterns in the nematode *Caenorhabditis elegans* (Fig 1A; Oren-Suissa *et al*, 2010; Smith *et al*, 2010; Albeg *et al*, 2011) to investigate the role of different classes of *N*-glycans during development. The intricately branched PVD neurons possess polymodal functions of proprioception, nociception, and mechanosensation (Chatzigeorgiou *et al*, 2010; Albeg *et al*, 2011; Cohen *et al*, 2014; Tao *et al*, 2019). We found that *aman-2/Golgi alpha-mannosidase* II, a conserved enzyme important for the synthesis of complex and paucimannose-type *N*-glycans, is required for PVD dendrite morphogenesis. Specifically, *aman-2/Golgi alpha-mannosidase II* allows for the proper decoration of the leucine-rich transmembrane receptor DMA-1/LRR-TM in PVD with the correct set of high-mannose/hybrid/paucimannose *N*-glycans on specific *N*-glycosylation sites. Rather than controlling trafficking or surface localization of DMA-1/LRR-TM, we provide evidence that the proper *N*-glycosylation of DMA-1/LRR-TM in PVD is essential for the function of DMA-1/LRR-TM as part of the Menorin pathway during PVD patterning. This pathway comprises two conserved cell adhesion molecules, SAX-7/L1CAM and MNR-1/Menorin, that function from the epidermis, and a secreted chemokine LECT-2/Chondromodulin II from muscle that, together with DMA-1/LRR-TM, form a high affinity cell adhesion complex (Fig 1B; Inberg *et al*, 2019; Sundararajan *et al*, 2019). Together, our experiments suggest that distinct classes of *N*-glycans, rather than *N*-glycosylation *per se*, serve specific functions in dendrite branching and contribute to developmental specificity during neuronal morphogenesis.

Results and Discussion

The *N*-glycosylation enzyme AMAN-2/Golgi alpha-mannosidase II is required for PVD dendrite patterning

To identify additional factors that regulate the Menorin pathway, we performed an unbiased genetic screen for factors that modify a partial loss of function allele of the chemokine *lect-2/Chondromodulin II* (Diaz-Balzac *et al*, 2016; Zou *et al*, 2016). We isolated *dz261* as a strong enhancer of the partial loss of function *lect-2* mutation in addition to other alleles in known genes of the Menorin pathway (Figs 1A and D, and EV1A–C). Using a combination of mapping, sequencing, and transformation rescue, we identified *dz261* as an allele of *aman-2/Golgi alpha-mannosidase II* (Figs 1C and EV1A–C), which encodes a central enzyme in the *N*-glycosylation biosynthetic pathway not previously implicated in dendrite development. The allele *dz261* is likely a complete loss of function mutation as it introduces an early stop codon in the key enzymatic domain of the protein (Figs 1C and EV1A–C). Quantifications of PVD branching patterns in *aman-2(dz261)* null mutants, as well as four additional nonsense/deletion alleles of *aman-2*, demonstrate that this Golgi alpha-mannosidase II is required for the formation of quaternary branches, but not for the formation of secondary or tertiary branches of PVD dendrites (Figs 1D and E, and EV1D). These observations are reminiscent of partial loss of function alleles of *dma-1/LRR-TM* (Tang *et al*, 2019) and suggest that *aman-2* may be necessary for full functionality of the Menorin pathway. Of note, we observed no obvious

Figure 1. AMAN-2/Golgi alpha-mannosidase II is required for PVD dendrite patterning.

A Fluorescent images (left panels) and tracings (right panels) of PVD neurons of the indicated genotypes. PVD is visualized by the *wdIs52* transgene. Primary (1°), secondary (2°), tertiary (3°), and quaternary (4°) dendrites are indicated, and the cell body is marked with an asterisk. Anterior is to the left and dorsal is up in all panels. Scale bars represent 20 μm.

B Schematic of the Menorin complex, including DMA-1/LRR-TM, SAX-7/L1CAM, MNR-1/Menorin, and LECT-2/Chondromodulin II, as well as the negative regulator KPC-1/Furin.

C Genomic environs of *aman-2*. An *N*-terminal transmembrane domain (TMD) is indicated, encoding a type II transmembrane protein. All alpha-mannosidase II proteins contain a glycosyl hydrolase 38 domain. Four nonsense alleles and one deletion allele (*tm1078)* of *aman-2* are denoted.

D Quantification of the number of quaternary branches (indicated in schematic) in different *aman-2* alleles and in wild-type control animals. All loss of function alleles of *aman-2* display a significant decrease in PVD quaternary branch number. Data are represented as mean ± SEM. Statistical significance was calculated using the Kruskal–Wallis test and is indicated (****$P \leq 0.0001$). $n = 15$ for all genotypes and are biological replicates.

E Quantification of the number of full tertiaries (marked by secondary and tertiary branches as shown in schematic) in the genotypes indicated. Data are represented as mean ± SEM. Statistical significance was calculated using the Kruskal–Wallis test and is indicated (****$P \leq 0.0001$, ns = not significant). $n = 15$ for all genotypes and are biological replicates.

F Fluorescent images and tracings of PVD in *mnr-1(dz213)* hypomorphic animals alone and in combination with an *aman-2(gk248486)* null mutant. The *dz213* introduces a L135F missense mutation in the DUF2181 domain of MNR-1/Menorin. PVD is visualized by the *dzIs53* transgene. The cell body is marked with an asterisk. Scale bars represent 20 μm.

G Quantification of the number of full tertiaries in genotypes indicated and traced in (F). The loss of *aman*-2 severely enhances the *mnr-1(dz213)* phenotype. Control indicates wild-type control animals as shown in (A). Data are represented as mean ± SEM. Statistical significance was calculated using the Mann–Whitney test and is indicated (****$P \leq 0.0001$, ns = not significant). $n > 23$ for all genotypes and are biological replicates.

H Fluorescent images and tracings of PVD in *kpc-1(dz254)* hypomorph animals alone and in combination with an *aman-2(gk248486)* null mutant. PVD is visualized by the *dzIs53* transgene. White arrows indicate self-avoidance defects in tertiary branches. Red arrows show gaps between tertiary branches (no self-avoidance defects). The cell body is marked with an asterisk. Scale bars represent 20 μm.

I Quantification of the percent of self-avoidance defects in genotypes indicated and traced in (G). Control indicates wild-type control animals as shown in (A). The loss of *aman*-2 suppresses defects in the *kpc-1(dz254)* phenotype. Data are represented as mean. Statistical significance was calculated using the Z-test and is indicated (****$P \leq 0.0001$). $n > 15$ for all genotypes and are biological replicates.

Source data are available online for this figure.

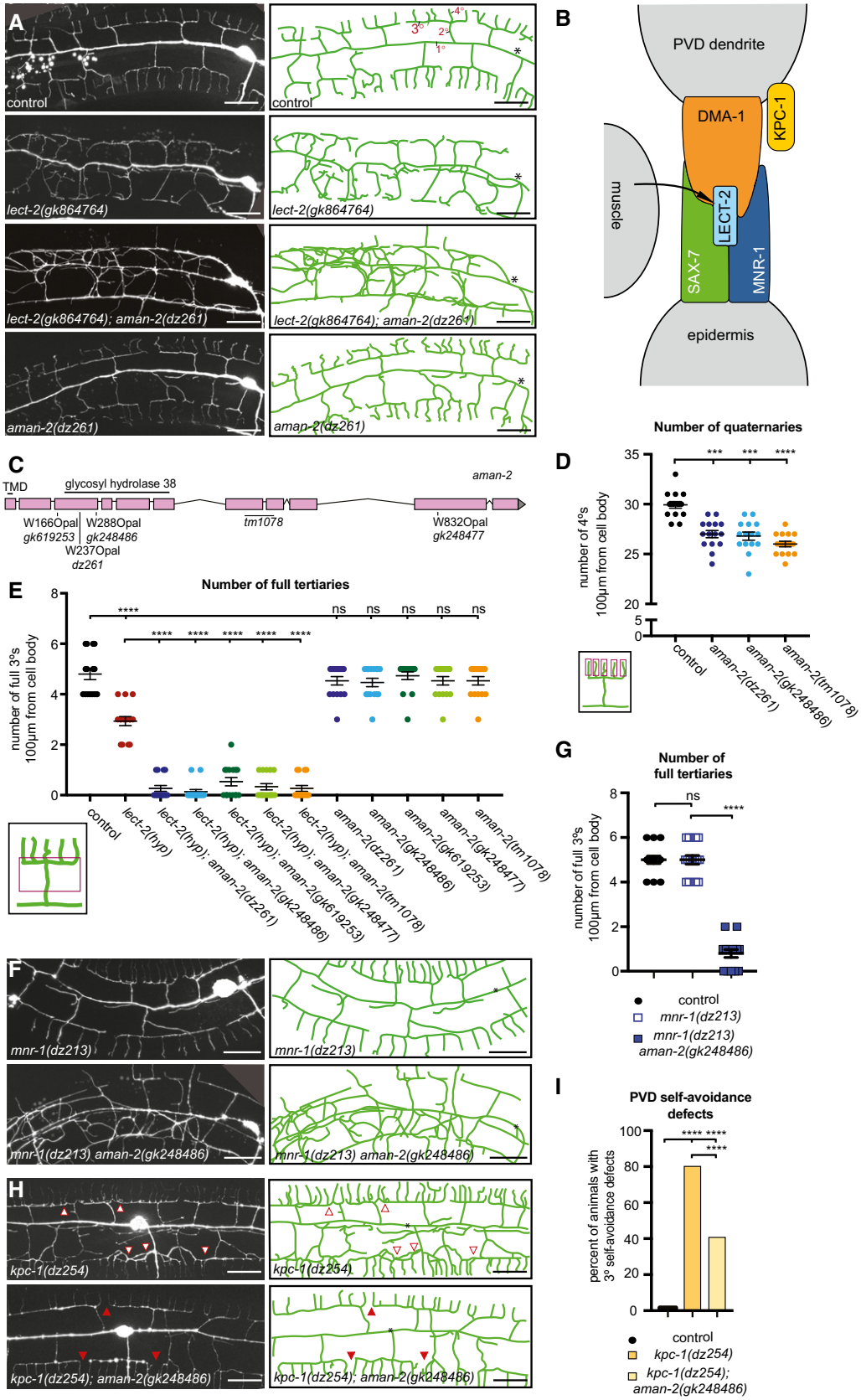
A
control
lect-2(gk864764)
lect-2(gk864764); aman-2(dz261)
aman-2(dz261)
B
PVD dendrite
DMA-1
KPC-1
LECT-2
SAX-7
MNR-1
muscle
epidermis
C
TMD
glycosyl hydrolase 38
aman-2
W166Opal gk619253
W288Opal gk248486
W237Opal dz261
tm1078
W832Opal gk248477
D
Number of quaternaries
number of 4°s 100µm from cell body
control
aman-2(dz261)
aman-2(gk248486)
aman-2(tm1078)
E
Number of full tertiaries
number of full 3°s 100µm from cell body
control
lect-2(hyp)
lect-2(hyp); aman-2(dz261)
lect-2(hyp); aman-2(gk248486)
lect-2(hyp); aman-2(gk619253)
lect-2(hyp); aman-2(gk248477)
lect-2(hyp); aman-2(tm1078)
aman-2(dz261)
aman-2(gk248486)
aman-2(gk619253)
aman-2(gk248477)
aman-2(tm1078)
F
mnr-1(dz213)
mnr-1(dz213) aman-2(gk248486)
G
Number of full tertiaries
number of full 3°s 100µm from cell body
control
mnr-1(dz213)
mnr-1(dz213) aman-2(gk248486)
H
kpc-1(dz254)
kpc-1(dz254); aman-2(gk248486)
I
PVD self-avoidance defects
percent of animals with 3° self-avoidance defects
control
kpc-1(dz254)
kpc-1(dz254); aman-2(gk248486)

Figure 1.

morphological phenotypes or defects in viability in animals lacking AMAN-2 (Fig EV1E).

AMAN-2/Golgi alpha-mannosidase II positively regulates the Menorin pathway

To directly test the genetic relationship between *aman-2/Golgi alpha-mannosidase II* and the Menorin pathway, we performed double mutant analyses. We found that the loss of *aman-2/Golgi alpha-mannosidase II* strongly enhances the severity of PVD branching defects in partial loss-of-function mutants of *lect-2/Chondromodulin II* (*gk864764)* and *mnr-1/Menorin* (*dz213*, Ramirez-Suarez & Bülow, unpublished) (Fig 1A and E–G), both of which are essential components of the conserved Menorin cell adhesion complex, and act as positive regulators of PVD development (Fig 1E–G; Dong *et al*, 2013; Salzberg *et al*, 2013; Diaz-Balzac *et al*, 2016; Zou *et al*, 2016). In contrast, the loss of *aman-2/Golgi alpha-mannosidase II* suppressed the self-avoidance defects of tertiary dendrites in a partial loss of function mutation of *kpc-1/Furin (dz254)* (Figs 1H and I, and EV1C), a known negative regulator of the Menorin pathway (Schroeder *et al*, 2013; Salzberg *et al*, 2014; Dong *et al*, 2016). Lastly, we found that a *dma-1; aman-2* double null mutant did not display a more severe dendrite phenotype than the *dma-1* mutant alone (Fig EV1F), suggesting that both genes function in a common pathway. We conclude that *aman-2/Golgi alpha-mannosidase II* normally functions to positively regulate the Menorin pathway to ensure correct PVD dendrite patterning.

AMAN-2/Golgi alpha-mannosidase II does not serve obvious functions in regulating transport or abundance of the DMA-1/LRR-TM

Mutations in *N*-glycosylation are often associated with protein folding defects and trafficking blocks due to misfolding (Stanley *et al*, 2015) and can, for example, result in lower abundance of cell surface proteins such as cell adhesion proteins in the nervous system (Medina-Cano *et al*, 2018). Because protein misfolding is more likely to occur at elevated temperatures (Gasser *et al*, 2008; Vabulas *et al*, 2010), we tested whether PVD branching defects in *aman-2/Golgi alpha-mannosidase II* mutants get progressively more severe with increasing temperatures. We found no significant increase in dendrite branching defects at 25°C compared to 15°C in *aman-2(gk248486)* mutant animals, in contrast to hypomorphic *lect-2(gk864764)* mutant animals (Fig EV2A and B). Previous work showed that mutations causing a secretory block as a result of a defective unfolded protein response trap a DMA-1::GFP reporter in the cell body of PVD (Wei *et al*, 2015; Salzberg *et al*, 2017). We therefore questioned whether the loss of *aman-2/Golgi alpha-mannosidase II* can lead to defects in protein folding and trafficking, and a possible secretory block. We analyzed the amount and number of puncta of the DMA-1::GFP reporter in the soma, as well as in dendrite branches, and found that DMA-1::GFP fluorescence in both the soma and primary dendrites, and the number of DMA-1::GFP puncta in tertiary dendrites, remained unaffected in *aman-2 (gk248486)* mutant animals (Fig EV2C–E). Moreover, localization or abundance of LECT-2/Chondromodulin II and SAX-7/L1CAM were also not obviously affected by loss of *aman-2/Golgi alpha-mannosidase II* (Fig EV2F and G). Taken together, these findings suggest that AMAN-2/Golgi alpha-mannosidase II may not primarily function to ensure protein folding, stability, or transport of factors of the Menorin pathway, but may rather regulate more specific aspects of the Menorin pathway during PVD patterning.

Enzymatic activity of AMAN-2/Golgi alpha-mannosidase II is required cell-autonomously in PVD to form higher order branches

The octasaccharide GnMan5Gn2 in a specific linkage configuration is the unique precursor to hybrid, complex, and paucimannose *N*-glycans (Fig 2A and B; Moremen, 2002; Paschinger *et al*, 2019). AMAN-2 is a Golgi alpha-mannosidase II, which is conserved from yeast to humans and cleaves two specific mannose residues from GnMan5Gn2, thereby generating the substrate for the formation of complex and paucimannose *N*-glycans (Fig 2A and B; Moremen, 2002; Paschinger *et al*, 2019). To determine where AMAN-2/Golgi alpha-mannosidase II functions and whether enzymatic activity is required for its role in PVD dendrite morphogenesis, we investigated transgenic expression of a wild-type AMAN-2 cDNA under the control of heterologous promoters in PVD, muscle, or epidermis for their ability to rescue *aman-2* mutant defects. Expression in PVD, but not muscle or epidermis, rescued the enhanced phenotypes in PVD dendrite branching of *lect-2(gk864764); aman-2(gk248486)* and *mnr-1(dz213) aman-2(gk248486)* double mutants (Fig 2C). These observations suggest that AMAN-2/Golgi alpha-mannosidase II functions cell-autonomously in PVD to pattern dendritic arbors.

Since AMAN-2/Golgi alpha-mannosidase II canonically functions as an enzyme (Moremen, 2002; Shah *et al*, 2008), we next asked whether catalytic activity is required for its role in PVD dendrite branching. We approached this both genetically and pharmacologically. Prior studies showed that two highly conserved aspartates are part of the conserved catalytic site in AMAN-2/Golgi alpha-mannosidases II (D306 and D443) and act sequentially to cleave off two mannose residues (Fig 2D; Shah *et al*, 2008). We found that an AMAN-2 cDNA with both aspartates mutated, and hence likely catalytically dead, failed to rescue the defects in *lect-2(gk864764); aman-2 (gk248486)* and *mnr-1(dz213) aman-2(gk248486)* double mutants (Fig 2C). To address the possibility that mutating the catalytic residues compromised the stability or structure of AMAN-2, we took advantage of swainsonine, a compound that specifically inhibits Golgi alpha-mannosidase II (Lu *et al*, 2014). We found that exposing animals to swainsonine resulted in PVD defects that were indistinguishable from the effects of a null mutation in *aman-2*, either in combination with a partial loss of function allele of *lect-2*, or in wild-type animals (Fig 2E–G). In other words, the pharmacological inhibition of AMAN-2/Golgi alpha-mannosidase II activity resulted in the same phenotypic consequences as genetically inactivating or removing the enzyme. Collectively, these findings lead us to conclude that the catalytic activity of AMAN-2/Golgi alpha-mannosidase II is essential to support dendrite patterning in PVD. This further implies that *N*-glycosylation of a molecule expressed in PVD is crucial for normal dendrite arborization.

The presence of abnormal *N*-glycans in *aman-2/Golgi alpha-mannosidase II* mutants results in defective PVD arborization

In eukaryotes, *N*-glycosylation is initiated in the endoplasmic reticulum (ER) with the synthesis of a 14-saccharide glycan on the

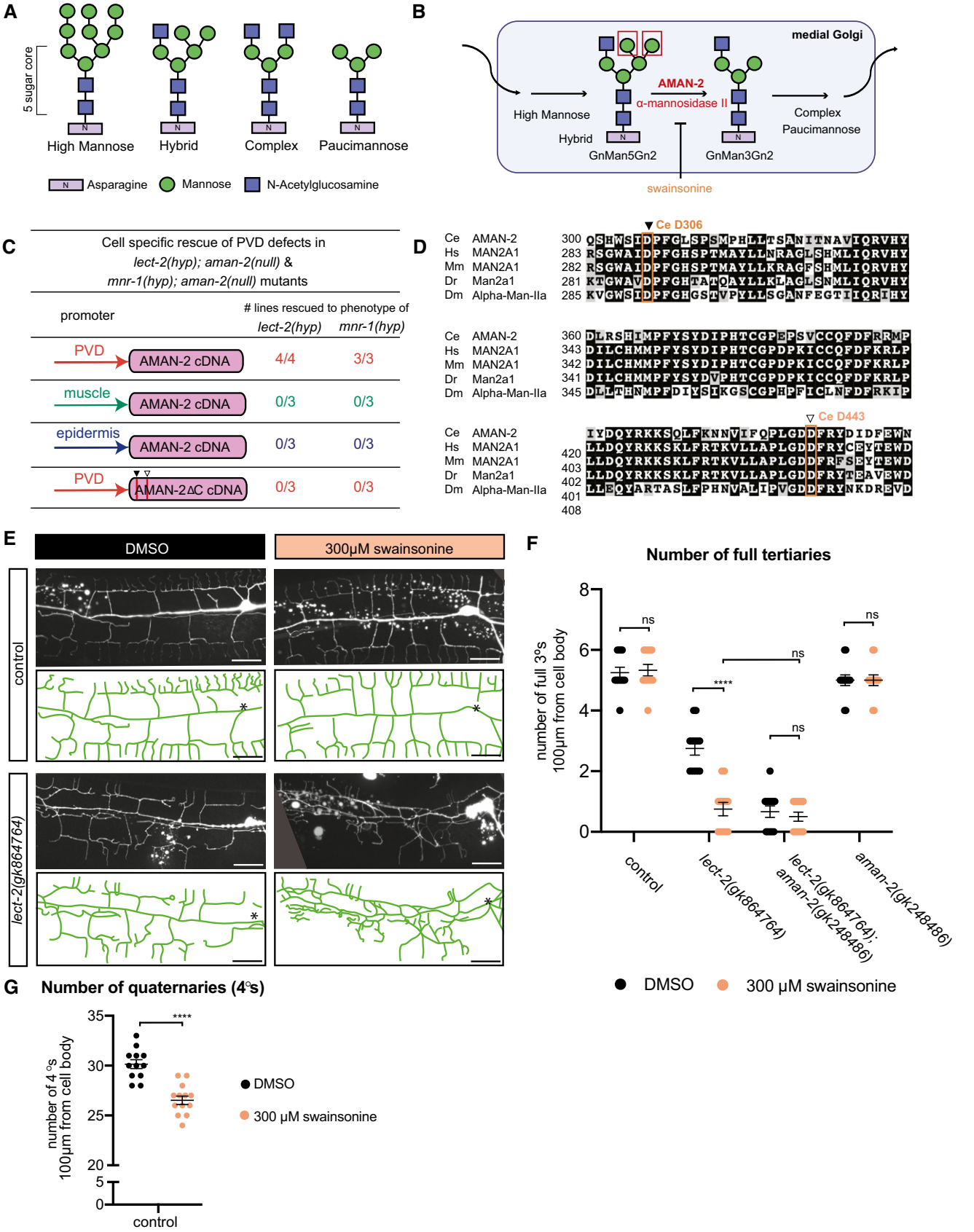
A
5 sugar core
High Mannose
Hybrid
Complex
Paucimannose
Asparagine
Mannose
N-Acetylglucosamine
B
medial Golgi
AMAN-2
α-mannosidase II
High Mannose
Hybrid
GnMan5Gn2
GnMan3Gn2
Complex
Paucimannose
swainsonine
C
Cell specific rescue of PVD defects in
lect-2(hyp); aman-2(null) &
mnr-1(hyp); aman-2(null) mutants
promoter
lines rescued to phenotype of
lect-2(hyp)
mnr-1(hyp)
PVD
AMAN-2 cDNA
4/4
3/3
muscle
AMAN-2 cDNA
0/3
0/3
epidermis
AMAN-2 cDNA
0/3
0/3
PVD
AMAN-2ΔC cDNA
0/3
0/3
D
Ce D306
Ce AMAN-2
Hs MAN2A1
Mm MAN2A1
Dr Man2a1
Dm Alpha-Man-IIa
300 QSHWSIDPFGLSPSMPHLLTSANITNAVIQRVHY
283 RSGWAIDPFGHSPTMAYLLNRAGLSHMLIQRVHY
282 RSGWAIDPFGHSPTMAYLLKRAGFSHMLIQRVHY
281 KTGWAVDPFGHTATQAYLLKLAGLSNMLIQRVHY
285 KVGWSIDPFGHGSTVPYLLSGANFEGTIIQRIHY
360 DLRSHIMPFYSYDIPHTCGPEPSVCCQFDFRRMP
343 DILCHMMPFYSYDIPHTCGPDPKICCQFDFKRLP
342 DILCHMMPFYSYDIPHTCGPDPKICCQFDFKRLP
341 DILCHMMPFYSYDVPHTCGPDPKICCQFDFKRLP
345 DLLTHNMPFDIYSIKGSCGPHPFLCLNFDFRKIP
Ce D443
420 IYDQYRKKSQLFKNNVIFQPLGDDFRYDIDFEWN
403 LLDQYRKKSKLFRTKVLLAPLGDDFRYCEYTEWD
402 LLDQYRKKSKLFRTKVLLAPLGDDFRFSEYTEWD
401 LLDQYRKKSKLFRTKVLLAPLGDDFRYTEAVEWD
408 LLEQYARTASLFPHNVALIPVGDDFRYNKDREVD
E
DMSO
300μM swainsonine
control
lect-2(gk864764)
F
Number of full tertiaries
number of full 3°s
100μm from cell body
ns
****
control
lect-2(gk864764)
aman-2(gk248486)
lect-2(gk864764);
aman-2(gk248486)
DMSO
300 μM swainsonine
G
Number of quaternaries (4°s)
number of 4°s
100μm from cell body
****
DMSO
300 μM swainsonine
control

Figure 2.

Figure 2. AMAN-2/Golgi alpha-mannosidase II requires enzymatic activity in PVD to form higher order branches.

A Types of *N*-linked glycans. The shared pentasaccharide core consists of two *N*-acetylglucosamines (blue squares) and 3 mannoses (green circles) attached onto an Asparagine residue with an N-X-S/T consensus site. Glycan types vary by identity of additional sugars onto the pentasaccharide core.

B Drawing showing the enzymatic activity of AMAN-2 in the medial Golgi. AMAN-2 cleaves two specific α1,3 and α1,6 mannose linked residues boxed in red, allowing for the formation of complex and paucimannose type *N*-glycans. Arrows denote other enzymes. Swainsonine specifically inhibits enzymatic activity of alpha-mannosidase II. (Man = mannose, Gn = *N*-acetylglucosamine).

C Table showing cell-specific rescue experiments of PVD defects. AMAN-2 cDNAs are expressed under the control of PVD, muscle, and epidermal specific promoters in the indicated double mutant backgrounds. Rescue is defined by restoration of the enhanced PVD phenotype back to that of the single hypomorphic mutants alone in aman-2(*gk248486)* null mutant backgrounds enhanced by *lect-2(gk846764)* or mnr-1(*dz213*). 25 transgenic animals and their non-transgenic siblings were scored for each line. Numbers indicate number of biological replicates that showed rescue.

D Multiple sequence alignment of human MAN2A1 (Hs; acc# NP_002363.2), mouse MAN2A1 (Mm; acc# NP_032575.2), zebrafish Man2a1 (Dr; acc# NP_001103497.2), fruit fly Alpha-Man-IIa (Dm; acc# NP_650494.2) and *C. elegans* AMAN-2 (Ce; acc# NP_505995.2) created by COBALT (constrained based multiple sequence alignment tool). Conserved catalytic sites D306 (black arrow) and D443 (white arrow) are boxed in orange.

E Fluorescent images and tracings of wild-type control (top) and *lect-2(gk846764)* hypomorphic animals (bottom) fed on plates with 300 μm swainsonine vs. a DMSO control. PVD is visualized by the *wyIs581* transgene. The cell body is denoted with an asterisk. Anterior is to the left and dorsal is up in all panels. Vesicular gut autofluorescence is visible as white circular staining. Scale bars represent 20 μm.

F Quantification of the number of full tertiaries in denoted genetic backgrounds (*aman-2* null is *gk248486)*. Black data points indicate DMSO and orange data points show swainsonine treated animals. Data are represented as mean ± SEM. Statistical significance was calculated using the Mann–Whitney test and is indicated (****$P \leq 0.0001$, ns = not significant). $n = 12$ for all genotypes and are biological replicates.

G Quantification of the number of quaternary dendrites in wild-type control animals fed on plates with and without 300 μm swainsonine. Animals treated with swainsonine show a significant decrease in quaternary branch number, akin to the data in Fig 1C. Data are represented as mean ± SEM. Statistical significance was calculated using the Mann–Whitney test and is indicated (****$P \leq 0.0001$). $n = 12$ for each experiment and are biological replicates.

Source data are available online for this figure.

phosphorylated polyisoprenol lipid dolichol-P-P (Stanley *et al*, 2015). Subsequently, the saccharide is transferred by a multiprotein complex termed oligosaccharyltransferase (OST) from dolichol-P-P to the aspartate within a N-X-S/T motif in nascent proteins as they are translocated into the ER (Stanley *et al*, 2015). As *N*-glycosylated proteins transit the Golgi, the glycans undergo a series of enzymatic modifications that add and remove specific sugar residues, leading to a wide array of possible *N*-glycan structures (Fig 3A; Stanley *et al*, 2015). For example, in one of the earlier steps, the enzyme MGAT1 adds a *N*-acetylglucosamine residue to Man5Gn2 to form GnMan5Gn2 (Fig 3A). Genetically removing MGAT1 in mice results in the complete loss of complex and hybrid *N*-glycans and early embryonic death, demonstrating that these *N*-glycans are essential for mammalian development (Ioffe & Stanley, 1994; Metzler *et al*, 1994). GnMan5Gn2 is the substrate for AMAN-2/MAN2A, which sequentially removes two mannose residues to form GnMan3Gn2 (Fig 3A) (Stanley *et al*, 2015). These reactions are followed by either removal or addition of additional sugars, or modification by a host of other conserved enzymes that lead to either complex or paucimannose *N*-glycans (Fig 3A). To determine which specific *N*-glycans are missing in *aman-2* mutants and are therefore required for normal branching of PVD dendrites, we systematically tested whether mutations in any of the genes downstream of *aman-2* (including *hex-2/hexosaminidase*, *hex-3/hexosaminidase*, *fut-8/FUT8 Fucosyltransferase*, and *gly-20/MGAT II*) would also enhance the *lect-2* partial loss of function allele. We found that removing the genes encoding these enzymes alone, or in combination, did not enhance the *lect-2* partial loss of function allele (Fig EV3A). Mutating MGAT1/*N*-acetylglucosaminyltransferase-I (in worms encoded by three paralogous genes *gly-12*, *gly-13*, *gly-14*) (Chen *et al*, 1999, 2003), which acts immediately before AMAN-2/Golgi alpha-mannosidase II, also showed no effects (Fig EV3B). Collectively, these findings suggest that no lack of specific *N*-glycans downstream of MGAT1, or of AMAN-2, alone are responsible for the observed defects in PVD dendrites.

Previous structural studies of *N*-glycans in *aman-2(tm1078)* null mutant animals (Paschinger *et al*, 2006) established that the loss of *aman-2/Golgi alpha-mannosidase II* in *C. elegans* caused (i) a loss of the normal products of AMAN-2, including complex *N*-glycans (Fig 3A, shaded in green) and (ii) a buildup of GnMan5Gn2, the substrate of AMAN-2 (Fig 3A; Paschinger *et al*, 2006). This GnMan5Gn2 intermediate was found to serve as substrate for other enzymes further downstream (including *FUT-8/Fut8 Fucosyltransferase* and *PCT*/Phosphorylcholine-transferase) leading to the appearance of abnormal *N*-glycans, not normally present in wild-type animals (Fig 3A, shaded in red) (Paschinger *et al*, 2006). To determine whether the defects in PVD branching were caused by the absence of wild-type *N*-glycans, or the presence of abnormal GnMan5Gn2 *N*-glycans, we mutated both MGAT1 and AMAN-2 in the partial loss of function backgrounds of *lect-2* and *mnr-1*. The prediction was that if the enhancement of the partial loss of function alleles of *lect-2* or *mnr-1* by the loss of *aman-2* is caused by abnormal *N*-glycans, then removal of MGAT1, the preceding enzyme would suppress that enhancement. Indeed, the loss of MGAT1 did suppress the enhanced phenotypes in *lect-2; aman-2* and *mnr-1; aman-2* double mutants (Fig 3B and C). Moreover, the decrease in quaternary PVD branches in AMAN-2 mutants is also suppressed by the loss of MGAT1 (Fig 3D). These data indicate that one or more structurally abnormal *N*-glycan(s) with a terminal *N*-acetylglucosamine introduced by MGAT1 are responsible for the observed defects in PVD patterning.

DMA-1/LRR-TM *N*-glycosylation is changed in *aman-2/Golgi alpha-mannosidase II* mutants

Since we demonstrated that (i) *aman-2/Golgi alpha-mannosidase II* genetically interacts with the Menorin pathway, and (ii) AMAN-2/Golgi alpha-mannosidase II activity is required cell-autonomously in PVD to regulate branching, we hypothesized that AMAN-2/Golgi alpha-mannosidase II directly regulates *N*-glycans on at least one

component of the Menorin complex in PVD. Treatment of whole worm lysates with the bacterial PNGase F glycosidase, which cleaves all *N*-glycans from Asn, resulted in distinct downward shifts in molecular weight of both DMA-1 and KPC-1, indicating that *N*-glycans were present on both proteins *in vivo* and had been removed (Figs 3E and EV4C). Thus, both PVD-expressed proteins,

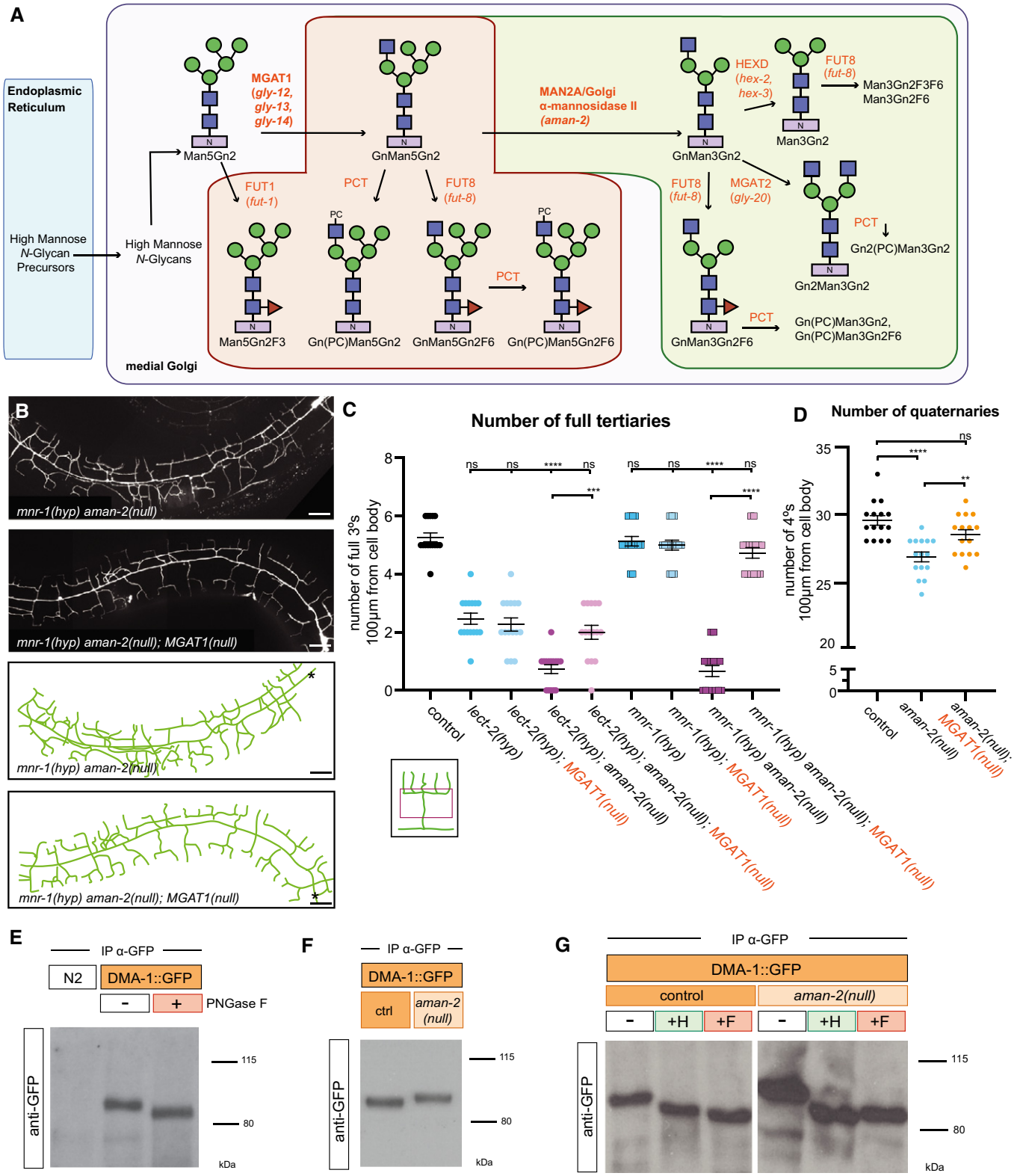

Figure 3.

Figure 3. The presence of abnormal *N*-glycans in mutants of AMAN-2/Golgi alpha-mannosidase II results in defects in PVD arborization.

A Schematic of the conserved *N*-glycosylation pathway in *C. elegans*. The blue box represents the Endoplasmic Reticulum, while the purple box represents the medial Golgi. Glycan residues are consistent with Fig 2A, with the addition of red triangles denoting fucose residues. Arrows and orange text represent enzymes. The green area marks wild-type *N*-glycan chains whereas the red area represents abnormal *N*-glycan chains that arise in the absence of AMAN-2. The glycans in the green area are not formed in the absence of AMAN-2. (Man = mannose, Gn = N-acetylglucosamine, F = fucose, PC = phosphorylcholine, MGAT1 = *N*-acetylglucosaminyltransferase I, FUT = fucosyltransferase, HEXD = hexosaminidase).

B Fluorescent composite images (top) and tracings (bottom) of *mnr-1(dz213)* in an *aman-2(gk248486)* and an *aman-2(gk248486); MGAT-1(null)* background. An MGAT null mutant lacks the three *C. elegans* paralogs: *gly-12*, *gly-13*, and *gly-14*. PVD is visualized by the *ωyIs581* transgene. The cell body is denoted with an asterisk. Anterior is to the left and dorsal is up in all panels. Scale bars represent 20 μm.

C Quantification of full tertiaries of denoted genotypes. Data are represented as mean ± SEM. Statistical comparisons were performed using the Kruskal–Wallis test. Statistical significance is indicated (***$P \leq 0.001$, ****$P \leq 0.0001$, ns = not significant). $n = 15$ for all genotypes and are biological replicates.

D Quantification of the number of quaternary branches in wild-type control, *aman-2(gk248486)* null, and *MGAT1(null)* animals. Loss of MGAT1 suppresses the decrease in quaternary branch number in the *aman-2(null)* background. Data are represented as mean ± SEM. Statistical significance was calculated using the Kruskal–Wallis test and is indicated (**$P \leq 0.01$, ****$P \leq 0.0001$). $n = 15$ for all genotypes and are biological replicates.

E Western blot against GFP in *C. elegans* lysate expressing no transgenes (N2) and expressing DMA-1::GFP (*qyIs369)*, after precipitating with anti-GFP antibody. The red boxed plus sign indicates that the lysate is treated with the PNGase F glycosidase. The downward size shift reveals that *N*-glycan structures are present on DMA-1. Ladder is marked in kilodaltons (kDa). The GFP tag contains no *N*-glycosylation sites. The experiment was repeated four times with biological replicates.

F Western blot against GFP in *C. elegans* lysate DMA-1::GFP (*qyIs369)*, after precipitating with anti-GFP antibody. Control indicates an otherwise wild-type background as opposed to an *aman-2(gk248486)* null background. The upward size shift in the mutant reveals that the loss of *aman-2* alters the identity of *N*-glycan structures on DMA-1. The experiment was repeated four times with biological replicates.

G Western blot against GFP in *C. elegans* lysate DMA-1::GFP (*qyIs369)*, after precipitating with anti-GFP antibody. Control indicates an otherwise wild-type background as opposed to an *aman-2(gk248486)* null background. The red boxed +F indicates that the lysate is treated with the PNGase F glycosidase, while the green boxed +H corresponds to the Endo H glycosidase, which cleaves high-mannose and hybrid type *N*-glycans. For complementary experiments using the Endo D glycosidase, which cleaves paucimannose type *N*-glycans, see Fig EV4B. Size shifts indicate that some hybrid/high-mannose structures are present on DMA-1 (left), and that the *aman-2* mutant results in only hybrid/high-mannose structures on DMA-1 (right). The experiment was repeated four times with biological replicates.

Source data are available online for this figure.

DMA/LRR-TM and KPC-1/Furin, are *N*-glycosylated, consistent with a previous report for DMA-1/LRR-TM (Feng *et al*, 2020). Another cell-autonomous factor and possible candidate, HPO-30/Claudin (Smith *et al*, 2013), contains no predicted *N*-glycan consensus motifs.

We next determined whether the loss of AMAN-2 resulted in altered *N*-glycosylation of DMA-1/LRR-TM. Interestingly, the absence of *aman-2/Golgi alpha-mannosidase II* resulted in a clear increase in DMA/LRR-TM molecular weight, whereas the size of KPC-1/Furin remained unaffected (Figs 3F and EV4C). The upward shift in the size of DMA-1/LRR-TM following the loss of *aman-2* is consistent with our genetic data establishing that the presence of abnormal GnMan5Gn2 *N*-glycans gives rise to the PVD mutant phenotype. To determine what types of *N*-glycans are attached to DMA-1 in wild-type and *aman-2* mutant backgrounds, we treated lysates with additional endoglycosidases: Endo H, which cleaves hybrid/high-mannose *N*-glycans, and Endo D, which cleaves only paucimannose *N*-glycans. Based on the size of the shifts observed, we conclude that in wild-type animals, DMA-1/LRR-TM possesses primarily hybrid/high-mannose *N*-glycans with a smaller amount of paucimannose *N*-glycans. In contrast, in the absence of AMAN-2, all *N*-glycans on DMA-1/LRR-TM were converted to hybrid/high-mannose type (likely GnMan5Gn2-derived *N*-glycans) with no or little detectable paucimannose *N*-glycans (Figs 3G and EV4A and B). Additionally, proteomic studies identified *C. elegans* SAX-7/L1CAM and LECT-2/Chondromodulin II as glycoproteins (Kaji *et al*, 2007), which we confirmed by a shift in molecular weight upon digestion of all *N*-glycans by PNGase F (Fig EV4D and E). However, in the absence of *aman-2/Golgi alpha-mannosidase II*, neither SAX-7/L1CAM and LECT-2/Chondromodulin II displayed obvious changes in molecular weight, suggesting that they may not carry abnormal *N*-glycans in an *aman-2* mutant background. Collectively, our data show that among the *N*-glycosylated proteins of the Menorin complex, only DMA-1/LRR-TM was significantly affected by the loss of *aman-2/Golgi alpha-mannosidase II* and carried altered *N*-glycans in *aman-2* null animals.

AMAN-2/Golgi alpha-mannosidase II modulates *N*-glycans on DMA-1/LRR-TM to regulate PVD morphogenesis

The DMA-1/LRR-TM receptor contains four predicted *N*-glycosylation motifs, all of which reside in leucine rich repeats (Fig 4A). To establish whether the *N*-glycosylation of DMA-1/LRR-TM is essential for its role in PVD dendrite branching, we mutated all four sites, alone and in combinations. Using CRISPR/Cas9-based genome editing, we converted the asparagine residues of the four predicted *N*-glycan attachment sites to glutamine to maintain chemical similarity, but eliminate the possibility of *N*-glycosylation. We cannot formally exclude that these mutations affect stability, transport or folding of the mutant DMA-1/LRR proteins, but consider this less likely, because these point mutants displayed different behaviors in different genetic backgrounds (see below). We found that only when abolishing predicted *N*-glycan attachment site 4 (N386), alone or in combination with other sites, was PVD quaternary branching compromised (Fig 4B). These results reveal that *N*-glycosylation of DMA-1/LRR-TM is required for its role in PVD patterning of quaternary branches and highlight the importance of N386 within a membrane proximal LRR repeat. We then assessed whether abolishing *N*-glycan attachment sites in an *aman-2/Golgi alpha-mannosidase II* loss of function background had any effects on dendrite patterning. Analysis of different site-specific mutations revealed that some *N*-glycosylation sites on DMA-1/LLR-TM enhance the severity of PVD dendrite branching defects in an *aman-2* mutant background (Fig 4C–E). The mutant phenotype resulting from a presumptive loss of all *N*-glycans on DMA-1 (S1234) is enhanced in an *aman-2* mutant background, suggesting that *N*-

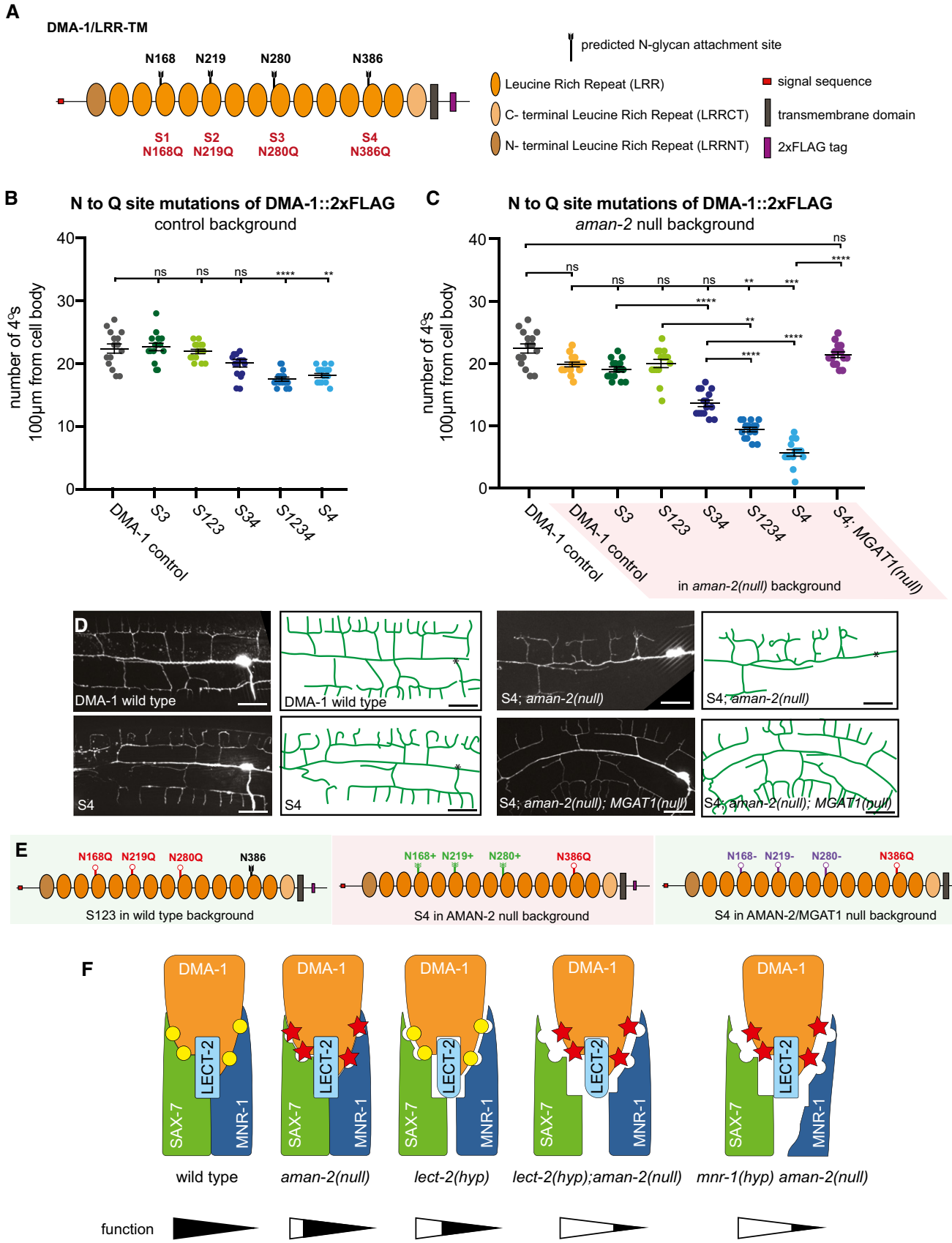
A
DMA-1/LRR-TM
N168
N219
N280
N386
S1 N168Q
S2 N219Q
S3 N280Q
S4 N386Q
predicted N-glycan attachment site
Leucine Rich Repeat (LRR)
C- terminal Leucine Rich Repeat (LRRCT)
N- terminal Leucine Rich Repeat (LRRNT)
signal sequence
transmembrane domain
2xFLAG tag
B
N to Q site mutations of DMA-1::2xFLAG
control background
number of 4°s 100µm from cell body
DMA-1 control
S3
S123
S34
S1234
S4
C
N to Q site mutations of DMA-1::2xFLAG
aman-2 null background
number of 4°s 100µm from cell body
DMA-1 control
DMA-1 control
S3
S123
S34
S1234
S4
S4; MGAT1(null)
in aman-2(null) background
D
DMA-1 wild type
DMA-1 wild type
S4; aman-2(null)
S4; aman-2(null)
S4
S4
S4; aman-2(null); MGAT1(null)
S4; aman-2(null); MGAT1(null)
E
N168Q N219Q N280Q N386
S123 in wild type background
N168+ N219+ N280+ N386Q
S4 in AMAN-2 null background
N168- N219- N280- N386Q
S4 in AMAN-2/MGAT1 null background
F
DMA-1
LECT-2
SAX-7
MNR-1
wild type
aman-2(null)
lect-2(hyp)
lect-2(hyp);aman-2(null)
mnr-1(hyp) aman-2(null)
function

Figure 4.

Figure 4. AMAN-2/Golgi alpha-mannosidase II modulates *N*-glycans on DMA-1/LRR-TM to regulate PVD morphogenesis.

A Schematic of DMA-1/LRR-TM with mutated *N*-glycan attachment sites S1-S4 indicated.

B Quantification of the number of quaternary branches in DMA-1::2xFLAG control animals and animals with combinations of DMA-1::2xFLAG *N*-glycan attachment sites mutated. Note that DMA-1::2xFLAG control animals display a slightly reduced number of quaternary dendrites compared to wild-type animals (Fig EV3C). Data are represented as mean ± SEM. Statistical significance was calculated using the Kruskal–Wallis test, and is indicated (**$P \leq 0.01$, ****$P \leq 0.0001$, ns = not significant). $n = 15$ for all genotypes and are biological replicates.

C Quantification of the number of quaternary branches in DMA-1::2xFLAG control animals alone and in combination with an *aman-2(gk248486)* null mutant (shaded in red). Control data is identical as in (B) and shown for comparison only. Data are represented as mean ± SEM. Statistical significance was calculated using the Kruskal–Wallis test and Mann–Whitney between individual comparisons, and is indicated (**$P \leq 0.01$, ***$P \leq 0.001$, ****$P \leq 0.0001$, ns = not significant). $n = 15$ for all genotypes and are biological replicates.

D Fluorescent images (left) and tracings (center) of PVD in animals of denoted backgrounds (*aman-2(null)* is *gk248486)*. S4 corresponds to the endogenous alteration of *N*-glycan attachment site N386 of DMA-1. PVD is visualized by the *dzIs117* transgene. The cell body is marked with an asterisk. Scale bars represent 20 μm.

E The schematics on the right detail the molecular context of the indicated backgrounds. Green indicates a relatively normal PVD structure and red a heavily defective arborization. Black attachments indicate wild-type, red indicate blocked sites, green indicates abnormal *N*-glycans chains, and purple indicates presumably incomplete but present *N*-glycan chains.

F Proposed model of how the function of the Menorin complex could be modulated by complex stability. Note that other mechanisms are possible (see discussion). Yellow circles represent normal *N*-glycan chains, while red stars represent abnormal *N*-glycans in *aman-2* mutant animals. Putative level of functionality is indicated below.

Source data are available online for this figure.

glycosylated proteins other than DMA-1/LRR-TM may serve additional functions during PVD morphogenesis, or that abnormal *N*-glycans on cryptic *N*-glycosylation sites further compromise function (Fig 4C). The results in an *aman-2* mutant background also suggest that having some type of *N*-glycan on site 4 of DMA-1/LRR-TM, even if abnormal, is better than having no *N*-glycan at all (cf. S4 and S123); second having such abnormal *N*-glycans on sites 1-3 further compromises DMA-1 function during PVD development (cf. S4 in control vs *aman-2* mutant background, Fig 4B–E). In line with the latter, we show that the loss of MGAT1 and AMAN-2 when site 4 of DMA-1 is mutant (S4), results in a suppression of the mutant quaternary phenotype (Fig 4C). This suggests that the presence of the abnormal *N*-glycans on sites 1-3, rather than 4, may be the major driver for the developmental defects in PVD dendrites. Of note, glycoproteomic studies in mammalian brains showed that different attachment sites in a given protein are not equal and can bear distinct *N*-glycans (Riley *et al*, 2019). While prior studies established the importance of *N*-glycosylation during neuronal development, our studies establish an important role for specific classes and structures of *N*-glycans in mediating neuronal development, and specifically dendrite patterning. They suggest that the DMA-1/LRR-TM receptor in PVD must be decorated with specific hybrid/high-mannose or paucimannose *N*-glycans as a result of AMAN-2 activity and that these specific *N*-glycans are important for Menorin complex function in PVD dendrite morphogenesis. A possible explanation is that the *N*-glycans on specific *N*-glycosylation sites in DMA-1/LRR-TM function permissively to maintain high affinity binding of DMA-1/LRR-TM to other members of the Menorin complex through specific *N*-glycans (Fig 4F). This interaction could be compromised by the formation of abnormal glycans in the absence of AMAN-2, leading to destabilization of the complex. Alternatively, the affinity of the proteins in the complex could be increased by different *N*-glycans, or modified in their function by other means. Regardless, our genetic and biochemical data, together with analytical data of *N*-glycans in *aman-2/Golgi alpha-mannosidase II* mutants (Paschinger *et al*, 2006), underscore the importance of AMAN-2/Golgi alpha-mannosidase II as a linchpin for the creation of complex and paucimannose *N*-glycans, and avoidance of abnormal hybrid and high-mannose-type *N*-glycans. Since metabolite availability can influence *N*-glycan synthesis and flux (reviewed in Dennis *et al*, 2009), these findings also raise the possibility that environmental factors can intersect with intrinsic genetic programs to regulate the function of extracellular adhesion complexes during neural development by modulating *N*-glycosylation. While AMAN-2 is most highly expressed in PVD neurons (CeNGEN; Taylor *et al*, 2021), it may be of interest to determine systematically whether it plays a role in the development of other neurons in which it is expressed.

Previous studies demonstrated that *N*-glycosylation is important for folding and surface localization of cell adhesion molecules and axon guidance factors in vertebrates and invertebrates, such as L1CAMs and ephrins, respectively (Sekine *et al*, 2013; Medina-Cano *et al*, 2018; Mire *et al*, 2018). On the other hand, structural studies and *in vitro* experiments suggested that *N*-glycans can regulate protein–protein interactions of cell adhesion molecules (Fogel *et al*, 2010; Labasque *et al*, 2014; Li *et al*, 2016). Our findings demonstrate *in vivo*, that not only *N*-glycans *per se*, but that specific classes of *N*-glycan structures are important to modulate cell-cell signaling, and possibly, receptor-ligand binding, complex formation, or function. This is reminiscent of the role of *O*-fucose glycans on the Notch receptor extracellular domain, which affect its signaling and ligand interactions (Moloney *et al*, 2000). Given that over 70% of proteins transiting the secretory pathway are *N*-glycosylated (Apweiler *et al*, 1999), these findings raise the possibility that specific *N*-glycan structures are important determinants to regulate the interactions of extracellular complexes during nervous system development more broadly, and could contribute to the specificity that is required in the nervous system of both vertebrates and invertebrates. In this context, it is interesting to note that over 70 congenital disorders of glycosylation affecting genes in the *N*-glycosylation pathway have been described (Freeze, 2006; Ng & Freeze, 2018), of which many are associated with intellectual disability or other neurological symptoms (Jaeken & Peanne, 2017; Chang *et al*, 2018). While no mutations in Golgi alpha-mannosidase II in humans have been described to date, it is conceivable that such mutations exist, and may result in neurological phenotypes. Our studies provide the conceptual framework for the investigation of developmental defects of the nervous system in mutants of genes involved in *N*-glycosylation and this growing class of congenital disorders.

Materials and Methods

Reagents and Tools table

Reagent/Resource	Source	Identifier/Catalog #
Bacterial and Virus strains		
Escherichia coli: OP50	Caenorhabditis Genetics Center	OP50
Experimental Models: Organisms/Strains		
C. elegans: *wild-type isolate*	Caenorhabditis Genetics Center	N2
C. elegans: *wdIs52 II*	Kind gift of David Miller	NC1687
C. elegans: *wyIs378 X*	Kind gift of Kang Shen	*wyIs378*
C. elegans: *wyIs581 IV*	Kind gift of Kang Shen	*wyIs581*
C. elegans: *dzIs117 II*	This paper	*dzIs117*
C. elegans: *lect-2(dz249[lect-2::mNeonGreen::3XFLAG]) II*	Diaz-Balzac *et al* (2016)	EB2724
C. elegans: *lect-2(dz249[lect-2::mNeonGreen::3XFLAG]) II; him-5(ok1896) V*	Diaz-Balzac *et al* (2016)	EB3894
C. elegans: *dzIs53 ddIs290 (SAX-7::GFP::3XFLAG) II; him-5(ok1896) V*	Diaz-Balzac *et al* (2016)	EB2808
C. elegans: *lect-2(dz249[lect-2::mNeonGreen::3XFLAG]) II; aman-2(dz261) V*	This paper	EB3185
C. elegans: *dzIs53 ddIs290 (SAX-7::GFP::3XFLAG) II; aman-2(dz261) V*	This paper	EB3182
C. elegans: *qyIs369 X*	Kind gift of Kang Shen	*qyIs369*
C. elegans: *wyIs581 IV; qyIs369 X*	This paper	EB3534
C. elegans: *wyIs581 IV; qyIs369 X; aman-2(gk248486) V*	This paper	EB3634
C. elegans: *dzIs53 II; him-5(ok1896) V*	This paper	EB2824
C. elegans: *lect-2(gk864764) II; wyIs378 X*	This paper	EB2795
C. elegans: *wdIs52 lect-2(gk864764) II*	This paper	EB2805
C. elegans: *kpc-1(dz254) I; wdIs52 lect-2(gk864764) II*	This paper	EB2908
C. elegans: *wdIs52 lect-2(gk864764) II; mnr-1(dz252) V*	This paper	EB2906
C. elegans: *wdIs52 lect-2(gk864764) II; sax-7(dz253) IV*	This paper	EB2907
C. elegans: *wdIs52 lect-2(gk864764) II; aman-2(dz261) V*	This paper	EB2915
C. elegans: *wyIs581 IV; him-5(ok1896) V*	This paper	EB2926
C. elegans: *kpc-1(dz254) I; dzIs53 II*	This paper	EB2983
C. elegans: *kpc-1(dz254) I; dzIs53 II; him-5(ok1896) V*	This paper	EB3282
C. elegans: *kpc-1(dz254) I; dzIs53 II; aman-2(gk248486) V*	This paper	EB3299
C. elegans: *lect-2(gk864764) II; wyIs581 IV; him-5(ok1896) V*	This paper	EB3061
C. elegans: *dzIs53 II; mnr-1(dz213) V*	This paper	EB3281
C. elegans: *wyIs581 IV; mnr-1(dz213) aman-2(gk248486) V*	This paper	EB3403
C. elegans: *aman-2(gk248486) V*	Caenorhabditis Genetics Center	VC20294
C. elegans: *aman-2(gk248477) V*	Caenorhabditis Genetics Center	VC20422
C. elegans: *aman-2(gk619253) V*	Caenorhabditis Genetics Center	VC40398
C. elegans: *aman-2(tm1078) V*	Kind gift of the Shohei Mitani	*tm1078*
C. elegans: *lect-2(gk864764) II; wyIs581 IV*	This paper	EB3228
C. elegans: *lect-2(gk864764) II; wyIs581 IV; aman-2(gk248486) V*	This paper	EB3260
C. elegans: *wyIs581 IV; aman-2(gk248486) V*	This paper	EB3261
C. elegans: *lect-2(gk864764) II; wyIs581 IV; aman-2(gk248477) V*	This paper	EB3293
C. elegans: *lect-2(gk864764) II; wyIs581 IV; aman-2(gk619253) V*	This paper	EB3294
C. elegans: *lect-2(gk864764) II; wyIs581 IV; aman-2(tm1078) V*	This paper	EB4422
C. elegans: *wyIs581 IV; aman-2(gk248477) V*	This paper	EB3405
C. elegans: *wyIs581 IV; aman-2(gk619253) V*	This paper	EB3406
C. elegans: *wyIs581 IV; aman-2(tm1078) V*	This paper	EB4183

Reagents and Tools table (continued)

Reagent/Resource	Source	Identifier/Catalog #
C. elegans: *dzIs117 II; him-5(ok1896) V*	This paper	EB3353
C. elegans: *pyc-1(gk689405) V*	Caenorhabditis Genetics Center	VC40551
C. elegans: *lect-2(gk864764) II; wyIs581 IV; pyc-1(gk689405) V*	This paper	EB3298
C. elegans: *gly-12(id47) X*	Caenorhabditis Genetics Center	AS270
C. elegans: *dpy-6(e14) gly-13(ok712) X*	Caenorhabditis Genetics Center	AS338
C. elegans: *gly-14(id48) III*	Caenorhabditis Genetics Center	AS271
C. elegans: *gly-14(id48) III; gly-12(id47) gly-13(ok712) X*	Kind gift of Iain Wilson	AS341
C. elegans: *gly-20(ok826) V*	Caenorhabditis Genetics Center	RB943
C. elegans: *fut-8(ok2558) V*	Caenorhabditis Genetics Center	RB1945
C. elegans: *hex-2(ok2985) V*	Caenorhabditis Genetics Center	RB2205
C. elegans: *hex-3(gk944651) III*	Caenorhabditis Genetics Center	VC40929
C. elegans: *lect-2(gk864764) II; wyIs581 IV; gly-12(id47) X*	This paper	EB3407
C. elegans: *lect-2(gk864764) II; wyIs581 IV; dpy-6(e14) gly-13(ok712) X*	This paper	EB3408
C. elegans: *wyIs581 IV; gly-20(ok826) V*	This paper	EB3410
C. elegans: *wyIs581 IV; fut-8(ok2558) V*	This paper	EB3411
C. elegans: *lect-2(gk864764) II; otIs173 III; wyIs581 IV; hex-2(ok2985) V*	This paper	EB3653
C. elegans: *lect-2(gk864764) II; hex-3(gk944651) III; wyIs581 IV; him-5(ok1896) V*	This paper	EB3905
C. elegans: *lect-2(gk864764) II; hex-3(gk944651) III; wyIs581 IV; hex-2(ok2985) V*	This paper	EB3906
C. elegans: *ddIs290 lect-2(gk864764) II; gly-14(id48) III; wyIs581 IV*	This paper	EB3638
C. elegans: *ddIs290 lect-2(gk864764) II; wyIs581 IV; gly-12(id47) gly-13(ok712) X*	This paper	EB3637
C. elegans: *ddIs290 lect-2(gk864764) II; gly-14(id48) III; wyIs581 IV; gly-12(id47) gly-13(ok712) X*	This paper	EB3636
C. elegans: *dzIs53 II; gly-14(id48) III; wyIs581 IV; mnr-1(dz213) V; gly-12(id47) gly-13(ok712) X*	This paper	EB4376
C. elegans: *dzIs53 II; gly-14(id48) III; wyIs581 IV; mnr-1(dz213) aman-2(gk248486) V; gly-12 (id47) gly-13(ok712) X*	This paper	EB4377
C. elegans: *dzIs117 II; gly-14(id48) III; wyIs581 IV; aman-2(gk248486) V; gly-12(id47) gly-13 (ok712) X*	This paper	EB4420
C. elegans: *dzEx1865(Pser-2prom3::kpc-1::GFP); dzIs53 I*	This paper	EB3533
C. elegans: *dzEx1865(Pser-2prom3::kpc-1::GFP); dzIs53 II; aman-2(gk248486) V*	This paper	EB3667
C. elegans: *dma-1(wy1041[dma-1::2XFLAG]) I; dzIs117 II*	This paper	EB4239
C. elegans: *dma-1(wy1041[dma-1::2XFLAG]) I; dzIs117 II; him-5(ok1896) V*	This paper	EB4378
C. elegans: *dma-1(dz294[dma-1(N280Q)::2xFLAG]) I; dzIs117 II; him-5(ok1896) V*	This paper	EB4219
C. elegans: *dma-1(dz294[dma-1(N280Q)::2xFLAG]) I; dzIs117 II; aman-2(gk248486) V*	This paper	EB4220
C. elegans: *dma-1(dz295[dma-1(N168Q, N219Q, N280Q)::2xFLAG]) I; dzIs117 II; him-5(ok1896) V*	This paper	EB4223
C. elegans: *dma-1(dz295[dma-1(N168Q, N219Q, N280Q)::2xFLAG]) I; dzIs117 II; aman-2 (gk248486) V*	This paper	EB4224
C. elegans: *dma-1(dz296[dma-1(N280Q; N386Q)::2xFLAG]) I; dzIs117 II; him-5(ok1896) V*	This paper	EB4227
C. elegans: *dma-1(dz296[dma-1(N280Q; N386Q)::2xFLAG]) I; dzIs117 II; aman-2(gk248486) V*	This paper	EB4228
C. elegans: *dma-1(dz297[dma-1(N168Q, N219Q, N280Q, N386Q)::2xFLAG]) I; dzIs117 II; him-5 (ok1896) V*	This paper	EB4231
C. elegans: *dma-1(dz297[dma-1(N168Q, N219Q, N280Q, N386Q)::2xFLAG]) I; dzIs117 II; aman-2 (gk248486) V*	This paper	EB4232
C. elegans: *dma-1(dz298[dma-1(N386Q)::2xFLAG]) I; dzIs117 II; him-5(ok1896) V*	This paper	EB4235
C. elegans: *dma-1(dz298[dma-1(N386Q)::2xFLAG]) I; dzIs117 II; aman-2(gk248486) V*	This paper	EB4236
C. elegans: *dma-1(dz298[dma-1(N386Q)::2xFLAG]) I; dzIs117 II; gly-14(id48) III; aman-2 (gk248486) V; gly-12(id47) gly-13(ok712) X*	This paper	EB4421

Reagents and Tools table (continued)

Reagent/Resource	Source	Identifier/Catalog #
Oligonucleotides		
Guide RNA for S1: N126 [TAATACGACTCACTATAGGATAGAGACAATGATCGCAGTTTTAGAGCT AGAAATAGCAAG]	This paper	oMR103
Guide RNA for S2: N219 [TAATACGACTCACTATAgTTCCAAGTTGACGGAGTTGGTTTTAGA GCTAGAAATAGCAAG]	This paper	oMR122
Guide RNA for S3: N280 [TAATACGACTCACTATAgTTCGTATTGCAAAATGCACGTTTT AGAGCTAGAAATAGCAAG]	This paper	oMR123
guide RNA for S4: N386 [TAATACGACTCACTATAgAATGTTCAATGAAATCAGGGTTTTAGA GCTAGAAATAGCAAG]	This paper	oMR124
Repair for S1: N126Q [CGAAGTAAATTTGTAGAAAGATCACTGATAGTATTCTGAGAGAGGGAC AGGGAGCGGAGAGCTCTAAGATATGTGAATACTCCAGTTGGAAGAAT]	This paper	oMR130
Repair for S2: N219Q [GTTTCTCAATTGGATGAATTATATTTGAATCATTGCCAGCTCTCCTCCATC TACTCCCTCGCACTCGACCGCATCCCTCAGCTGCGCCAGCTGGGAATCGGAGGAAATAATCTCAA AATGGTTCCAAC]	This paper	oMR131
Repair for S3: N280Q [CCGAGCAAATTGTGGGAAAGATCTAATTTTGAGATCTGCGTATTGCAA AATGCACAAGCTGTGATTTCTTGAATGGAATTGTGAGACAAGTC]	This paper	oMR127
Repair for S4: N386Q [TTGTCAGGCAAATAAGTCAATTCATTTCCAGAAATCTGCAGTGAGATGAGG TGATAATAGCGAGACGGCAGCTGTACCGGGATGAATTT]	This paper	oMR132
Genotype S1 forward [GAGTTCTTCGTCTCATCAATTG]	This paper	oMR107
Genotype S1 reverse [GAATAGGATTCCGGTCTAGTCG]	This paper	oMR108
Genotype S2, S3 forward [CTGCGATCATTGTCTCTATCC]	This paper	oMR109
Genotype S2 reverse [CCATCCCAACCATTTTGAGTC]	This paper	oMR129
Genotype S3 reverse [GGTCCATGACTCCTCGAAA]	This paper	oMR111
Genotype S4 forward [GCACATGAACAATCCCAAGG]	This paper	oMR112
To clone *Pser2prom3*::*aman-2*, *Pdpy-7*::*aman-2*, *Pmyo-3*::*aman-2* forward [TTCAGGAGGACCCTTGGAGGGTACcATGGGAAAACGCAATTTCTATATTATCCTA]	This paper	oMR34
To clone *Pser2prom3*::*aman-2*, *Pdpy-7*::*aman-2*, *Pmyo-3*::*aman-2* reverse [GATATTTCCAGTATTCTTGTATCATTTTAAtCCGGAACCCGCCTTTGTCTGATCT]	This paper	oMR35
To clone *Pser2prom3*::*aman-2 catalytic dead* site 1 forward [CATTGGTCAATTGCCC CATTCGGTTTATC]	This paper	oMR64
To clone *Pser2prom3*::*aman-2 catalytic dead* site 1 reverse [GATAAACCGAATGGGGCAAT TGACCAATG]	This paper	oMR65
To clone *Pser2prom3*::*aman-2 catalytic dead* site 2 forward [CCACTTGGAGATGCCTTC AGGTACGAC]	This paper	oMR66
To clone *Pser2prom3*::*aman-2 catalytic dead* site 2 reverse [GTCGTACCTGAAGGCAT CTCCAAGTGG]	This paper	oMR67
Recombinant DNA		
Plasmid: *Pser2prom3*::*aman-2*	The *aman-2* cDNA was PCR amplified with KpnI/BspeI cloning sites attached and cloned into *Pser2prom3*::*lect-2*.	N/A
Plasmid: *Pdpy-7*::*aman-2*	The *aman-2 cDNA* from *Pser2prom3*::*aman-2* was cloned into *Pdpy-7*::*lect-2* with KpnI/BspeI.	N/A
Plasmid: *Pmyo-3*::*aman-2*	The *aman-2cDNA* from *Pser2prom3*::*aman-2* was cloned into *Pmyo-3*::*lect-2* with KpnI/ BspeI.	N/A
Plasmid: *Pser2prom3*::*aman-2 catalytic dead*	The *Pser2prom3*::*aman-2* was PCR amplified with the NEB Q5 site directed mutagenesis kit.	N/A

Reagents and Tools table (continued)

Reagent/Resource	Source	Identifier/Catalog #
Endoglycosidases		
PNGase F (#P0704S)	NEB https://www.neb.com/products/p0704-pngase-f#Product%20Information	P0704S
Endo H (#P0702L)	NEB https://www.neb.com/products/p0702-endo-h#Product%20Information	P0702L
Endo D (#P0742S)	NEB https://www.neb.com/products/p0742-remove-it-endo-d#Product%20Information	P0742S
Antibodies		
Monoclonal primary Anti-GFP in mouse (Roche 11814460001)	Roche https://www.sigmaaldrich.com/US/en/product/roche/11814460001	11814460001
Monoclonal primary Anti-FLAG in mouse (Sigma F1804)	Sigma https://www.sigmaaldrich.com/US/en/product/sigma/f1804	F1804
Polyclonal secondary Anti-mouse HRP (Millipore AP308P)	Millipore https://www.emdmillipore.com/US/en/product/Goat-Anti-Mouse-IgG-Antibody-H+L-HRP-conjugate,MM_NF-AP308P	AP308P
Western Blot reagents		
4–12% Bis-Tris Gradient Gels	GenScript https://www.genscript.com/molecule/M00653-SurePAGE_Bis_Tris_10x8_4_12_12_wells.html	M00653
Protein A/G agarose beads (sc-2003)	Santa Cruz https://www.scbt.com/p/protein-a-g-plus-agarose	Sc-2003
Software and Algorithms		
Fiji	https://fiji.sc/	N/A
GraphPad PRISM 8	https://www.graphpad.com/scientific-software/prism/	N/A

Methods and Protocols

Caenorhabditis elegans handling

All strains were maintained using standard methods (Brenner, 1974) and experiments were performed at 20°C, except where indicated otherwise. Phenotypic analysis was performed in 1-day-old adults, with no more than 4–5 eggs present. Brood size was determined by single picking late L4 adults and allowing them to lay eggs on seeded plates for 48 h. Number of L1 larvae were subsequently counted per plate. For details and a complete list of strains used and generated in this study, see resources table.

Details of genetic screen and mutant alleles

The *lect-2(gk864764)* hypomorphic strain was treated with EMS (Kutscher & Shaham, 2014) and the progeny of clonal F1 animals scored for enhancement, suppression, or modification of the PVD branching phenotype. This screen resulted in the isolation of four mutant alleles (Fig EV1A). Guided by the phenotypes of *dz252*, *dz253*, and *dz254*, we used complementation tests and Sanger sequencing to identify the molecular lesions. For *dz261*, we used a combination of whole genome sequencing and single nucleotide polymorphism mapping (Minevich *et al*, 2012) to narrow down the region to a 5 Mb interval (11MB-16Mb) on chromosome V (Fig EV1B). This region contained 7 polymorphisms with predicted functional consequences. We injected seven fosmids covering those genes in pools and found that only the pool which contained a fosmid covering *aman-2* resulted in rescue (Fig EV1B). In addition, we obtained three nonsense alleles of *aman-2* (*gk248486*, *gk248477*, *gk619253*) from the Million Mutation Project (Thompson *et al*, 2013) and one deletion allele (*tm1078*, kind gift from the Mitani lab). The *dz261* mutation was further confirmed by Sanger sequencing of the original isolate, identifying a W237Opal nonsense mutation in the *aman-2* locus.

Molecular biology and transgenesis

To assemble tissue specific expression constructs used for heterologous rescue experiments, the *aman-2* cDNA clone *yk11g705*

(kind gift of Yoji Kohara) was cloned under control of the following promoters: PVD *ser2prom-3* (Tsalik *et al*, 2003), hypodermal *dpy-7p* (Gilleard *et al*, 1997), body wall muscle *myo-3p* (Okkema *et al*, 1993). These constructs were injected into N2 animals at 5 ng/µl, together with *myo-2p::mCherry* as an injection marker at 50 ng/µl and *BlueScript* as DNA filler up to a final DNA concentration of 100 ng/µl. Males from transgenic lines were then crossed into *lect-2(gk864764) II; wyIs581 IV; aman-2(gk248477)V* and *wyIs581 IV; mnr-1(dz213) aman-2(gk248486) V*. Point mutants in the *aman-2* cDNA were introduced by site-specific mutagenesis (NEB Q5 Site-Directed Mutagenesis). All plasmids contained the *unc-54* 3'UTR.

Pharmacology

Experiments in which the activity of AMAN-2 was blocked pharmacologically were performed with the compound swainsonine (1 mg swainsonine #16860 vials, Fisher Scientific catalog #NC1670046). Dosage experiments were performed from 50–500 µM of swainsonine dissolved in agar of NGM plates, with 300 µM being sufficient to elicit phenotypes in PVD. After drying agar plates for 24 h, 200 µl of OP50 *E. coli* was seeded onto each plate, and 5 young adult worms were left to self-fertilize and lay eggs. The F1 generations were analyzed, imaged, and quantified. DMSO was used as a control in plates not treated with swainsonine.

Western blot analysis and immunoprecipitation

Whole *C. elegans* lysates were generally prepared in RIPA buffer and sonicated in a Biorupter benchtop waterbath sonicator for 15 min. If applicable, lysates were treated with 1 unit of endoglycosidases PNGase F, Endo H, or Endo D, respectively, at temperatures as indicated in NEB protocols (linked in the Reagents and Tools table). Overnight immunoprecipitation of lysates with anti-GFP antibody prior to SDS–PAGE was performed for proteins with low expression levels (DMA-1::GFP and KPC-1::GFP) as follows. Five full plates of DMA-1::GFP and KPC-1::GFP tagged worms were washed in RIPA buffer pH7.0 and lysed for 15 min in a Biorupter water bath as previously described for whole worm protein extraction (Li & Zinovyeva, 2020). Post lysis, 20 uL of Protein A/G Plus Agarose beads (Santa Cruz sc-2003) and 1 µl of anti-GFP antibody (Roche 11814460001) were used to pull down DMA-1::GFP and KPC-1::GFP overnight at 4°C. For SAX-7::GFP::FLAG and LECT-2::mNG::FLAG, ten and twenty gravid adult animals, respectively, were sufficient to see robust expression on Western Blot without the necessity for precipitation. These samples were boiled and loaded directly into the gels. Gradient gels (4–12% GenScript) were used in all experiments. For all anti-FLAG blots, a concentration of 1:800 anti-Flag (Sigma F1804) and 1:5,000 anti-mouse HRP (Millipore AP308P) were used. For all anti-GFP blots, a concentration of 1:500 anti-GFP (Roche 11814460001) and 1:5,000 anti-mouse HRP (Millipore AP308P) was used.

CRISPR/Cas9 mediated gene editing

CRISPR-Cas9 constructs were designed and the *dpy-10* co-crispr protocol was followed as previously described (Dickinson & Goldstein, 2016) to introduce single point mutations of predicted *N*-glycan attachment Asparagine residues. Predicted sites were identified using NetNGlyc 1.0 Server (Gupta & Brunak, 2002). A battery of guideRNAs were designed to direct Cas9 cuts near sites of interest, and homologous repair template oligomers were designed to mutate Asparagine residues to Glutamine. Strains with combinations of mutated sites were generated by sequential injections and/or multiple simultaneous edits. Note, that all edits were made in strains with the C-terminus of DMA-1 already tagged with a 2XFLAG immunotag before the PDZ binding domain (Dong *et al*, 2016). Strains EB4219 through EB4238 in the Reagents and Tools table were obtained using these methods.

Imaging

Fluorescent images were captured in live *C. elegans* using a Plan-Apochromat 40×/1.4 or 63x/1.4 objective on a Zeiss Axioimager Z1 Apotome. Worms were immobilized using 1 mM Levamisole and *Z* stacks were collected. Maximum intensity projections were used for further analysis and tracing of dendrites. For quantification of branching, 1-day-old adults were mounted onto slides and immobilized with 1mM Levamisole. In both cases of capturing images and counting live on the microscope, the number of secondary and tertiary branches, "Os," (self-avoidance defects), and/or quaternary branches within 100 µm of the primary branch anterior to the cell body were quantified.

Quantification and statistical analysis

For quantifications of PVD branching, the experimenter was blinded to genotypes of point mutants in *dma-1*. Blinding for other genotypes was not possible, because genotypes could be inferred from phenotype. Statistical comparisons were conducted on Prism 8 GraphPad Software using Mann–Whitney, Kruskal–Wallis with Dunn's Multiple Comparison ad-hoc, Z-, or two-sided ANOVA with Dunnett's Multiple Comparison ad-hoc tests as appropriate. Statistical significance is indicated as ns, not significant; $*P \leq 0.05$; $**P \leq 0.01$; $***P \leq 0.001$ and $****P \leq 0.0001$.

Data availability

This study includes no data deposited in external repositories.

Expanded View for this article is available online.

Acknowledgements

We thank Scott Garforth, Sarah Garrett, Peri Kurshan, Yehuda Salzberg, Pamela Stanley, Robert Townley, and members of the Bülow laboratory for comments on the manuscript or helpful discussions during the course of this work. We thank David Miller, Shohei Mitani, Kang Shen, and Iain Wilson for reagents, and Yuji Kohara for the *yk11g705* cDNA clone. We are grateful to Meera Trivedi for sharing the *dzIs117* strain prior to publication. Some strains were provided by the Caenorhabditis Genome Center (funded by the NIH Office of Research Infrastructure Programs P40 OD010440). This work was supported by grants from the National Institute of Health (NIH): R01NS096672 and R21NS111145 to HEB; F31NS100370 to MR; T32GM007288 and F31HD066967 to CADB; P30HD071593 to Albert Einstein College of Medicine. We acknowledge support to MR by the Department of Neuroscience. NJRS was the recipient of a Colciencias-Fulbright Fellowship and HEB of an Irma T. Hirschl/Monique Weill-Caulier research fellowship.

Author contributions

Maisha Rahman: Conceptualization; Data curation; Formal analysis; Funding acquisition; Investigation; Visualization; Methodology; Writing—original draft; Writing—review and editing. **Nelson J Ramirez-Suarez:** Resources; Funding acquisition; Writing—review and editing. **Carlos A Diaz-Balzac:** Resources;

Funding acquisition; Writing—review and editing. **Hannes E Bülow:** Conceptualization; Formal analysis; Supervision; Funding acquisition; Validation; Visualization; Project administration; Writing—review and editing.

In addition to the CRediT author contributions listed above, the contributions in detail are:

Conceptualization Ideas: MR, HEB; Validation: MR; Formal Analysis: MR, HEB; Investigation: MR; Resources: NJR-S, CAD-B; Writing – Original Draft: MR; Writing – Review & Editing: MR, NJR-S, CAD-B, HEB; Visualization Preparation: MR; Project Administration: HEB; Funding Acquisition: MR, NJR-S, CAD-B, HEB.

Disclosure and competing interests statement

The authors declare that they have no conflict of interest.

References

Albeg A, Smith CJ, Chatzigeorgiou M, Feitelson DG, Hall DH, Schafer WR, Miller III DM, Treinin M (2011) *C. elegans* multi-dendritic sensory neurons: morphology and function. *Mol Cell Neurosci* 46: 308 – 317

Apweiler R, Hermjakob H, Sharon N (1999) On the frequency of protein glycosylation, as deduced from analysis of the SWISS-PROT database. *Biochim Biophys Acta* 1473: 4 – 8

Brenner S (1974) The genetics of *Caenorhabditis elegans*. *Genetics* 77: 71 – 94

Bülow HE, Hobert O (2006) The molecular diversity of glycosaminoglycans shapes animal development. *Ann Rev Cell Dev Biol* 22: 375 – 407

Chang IJ, He M, Lam CT (2018) Congenital disorders of glycosylation. *Ann Transl Med* 6: 477

Chatzigeorgiou M, Yoo S, Watson JD, Lee W-H, Spencer WC, Kindt KS, Hwang SW, Miller III DM, Treinin M, Driscoll M *et al* (2010) Specific roles for DEG/ENaC and TRP channels in touch and thermosensation in *C. elegans* nociceptors. *Nat Neurosci* 13: 861 – 868

Chen S, Spence Andrew M, Schachter H (2003) Isolation of null alleles of the *Caenorhabditis elegans* gly-12, gly-13 and gly-14 genes, all of which encode UDP-GlcNAc: α-3-D-mannoside β1,2-N-acetylglucosaminyltransferase I activity. *Biochimie* 85: 391 – 401

Chen S, Zhou S, Sarkar M, Spence AM, Schachter H (1999) Expression of three *Caenorhabditis elegans* N-acetylglucosaminyltransferase I genes during development. *J Biol Chem* 274: 288 – 297

Cohen E, Chatzigeorgiou M, Husson SJ, Steuer-Costa W, Gottschalk A, Schafer WR, Treinin M (2014) *Caenorhabditis elegans* nicotinic acetylcholine receptors are required for nociception. *Mol Cell Neurosci* 59: 85 – 96

Dennis JW, Nabi IR, Demetriou M (2009) Metabolism, cell surface organization, and disease. *Cell* 139: 1229 – 1241

Diaz-Balzac CA, Rahman M, Lazaro-Pena MI, Martin Hernandez LA, Salzberg Y, Aguirre-Chen C, Kaprielian Z, Bülow HE (2016) Muscle- and skin-derived cues jointly orchestrate patterning of somatosensory dendrites. *Curr Biol* 26: 2379 – 2387

Dickinson DJ, Goldstein B (2016) CRISPR-based methods for *Caenorhabditis elegans* genome engineering. *Genetics* 202: 885 – 901

Doitsidou M, Jarriault S, Poole RJ (2016) Next-generation sequencing-based approaches for mutation mapping and identification in *Caenorhabditis elegans*. *Genetics* 204: 451 – 474

Dong X, Chiu H, Park YJ, Zou W, Zou Y, Ozkan E, Chang C, Shen K (2016) Precise regulation of the guidance receptor DMA-1 by KPC-1/Furin instructs dendritic branching decisions. *Elife* 5: e11008

Dong X, Liu OW, Howell AS, Shen K (2013) An extracellular adhesion molecule complex patterns dendritic branching and morphogenesis. *Cell* 155: 296 – 307

Dong X, Shen K, Bülow HE (2015) Intrinsic and extrinsic mechanisms of dendritic morphogenesis. *Annu Rev Physiol* 77: 271 – 300

Feng Z, Zhao Y, Li T, Nie W, Yang X, Wang X, Wu J, Liao J, Zou Y (2020) CATP-8/P5A ATPase regulates ER processing of the DMA-1 receptor for dendritic branching. *Cell Rep* 32: 108101

Fogel AI, Li Y, Giza J, Wang Q, Lam TT, Modis Y, Biederer T (2010) N-glycosylation at the SynCAM (synaptic cell adhesion molecule) immunoglobulin interface modulates synaptic adhesion. *J Biol Chem* 285: 34864 – 34874

Freeze HH (2006) Genetic defects in the human glycome. *Nat Rev Genet* 7: 537 – 551

Gasser B, Saloheimo M, Rinas U, Dragosits M, Rodríguez-Carmona E, Baumann K, Giuliani M, Parrilli E, Branduardi P, Lang C *et al* (2008) Protein folding and conformational stress in microbial cells producing recombinant proteins: a host comparative overview. *Microb Cell Fact* 7: 11

Gilleard JS, Barry JD, Johnstone IL (1997) cis regulatory requirements for hypodermal cell-specific expression of the *Caenorhabditis elegans* cuticle collagen gene dpy-7. *Mol Cell Biol* 17: 2301 – 2311

Gupta R, Brunak S (2002) Prediction of glycosylation across the human proteome and the correlation to protein function. *Pac Symp Biocomput* 2002: 310 – 322

Hanus C, Geptin H, Tushev G, Garg S, Alvarez-Castelao B, Sambandan S, Kochen L, Hafner AS, Langer JD, Schuman EM (2016) Unconventional secretory processing diversifies neuronal ion channel properties. *Elife* 5: e20609

Holt CE, Dickson BJ (2005) Sugar codes for axons? *Neuron* 46: 169 – 172

Inberg S, Meledin A, Kravtsov V, Iosilevskii Y, Oren-Suissa M, Podbilewicz B (2019) Lessons from worm dendritic patterning. *Annu Rev Neurosci* 42: 365 – 383

Ioffe E, Stanley P (1994) Mice lacking N-acetylglucosaminyltransferase I activity die at mid-gestation, revealing an essential role for complex or hybrid N-linked carbohydrates. *Proc Natl Acad Sci USA* 91: 728 – 732

Jaeken J, Peanne R (2017) What is new in CDG? *J Inherit Metab Dis* 40: 569 – 586

Jan YN, Jan LY (2010) Branching out: mechanisms of dendritic arborization. *Nat Rev Neurosci* 11: 316 – 328

Kaji H, Kamiie J, Kawakami H, Kido K, Yamauchi Y, Shinkawa T, Taoka M, Takahashi N, Isobe T (2007) Proteomics reveals N-linked glycoprotein diversity in *Caenorhabditis elegans* and suggests an atypical translocation mechanism for integral membrane proteins. *Mol Cell Proteomics* 6: 2100 – 2109

Kutscher LM, Shaham S (2014) Forward and reverse mutagenesis in *C. elegans*. *WormBook* 1 – 26 https://doi.org/10.1895/wormbook.1.167.1

Labasque M, Hivert B, Nogales-Gadea G, Querol L, Illa I, Faivre-Sarrailh C (2014) Specific contactin N-glycans are implicated in neurofascin binding and autoimmune targeting in peripheral neuropathies. *J Biol Chem* 289: 7907 – 7918

Lefebvre JL (2021) Molecular mechanisms that mediate dendrite morphogenesis. In *Current Topics in Developmental Biology*, Bashaw GJ (ed), Vol. 142, pp 233 – 282. Cambridge, MA: Academic Press

Li L, Zinovyeva AY (2020) Protein extract preparation and co-immunoprecipitation from *Caenorhabditis elegans*. *J Vis Exp* https://doi.org/10.3791/61243

Li SA, Cheng L, Yu Y, Wang JH, Chen Q (2016) Structural basis of Dscam1 homodimerization: insights into context constraint for protein recognition. *Sci Adv* 2: e1501118

Lu H, Wang S-S, Wang W-L, Zhang L, Zhao B-Y (2014) Effect of swainsonine in *Oxytropis kansuensis* on Golgi α-mannosidase II expression in the brain tissues of Sprague-Dawley rats. *J Agric Food Chem* 62: 7407 – 7412

Masu M (2016) Proteoglycans and axon guidance: a new relationship between old partners. *J Neurochem* 139(Suppl 2): 58 – 75

Medina-Cano D, Ucuncu E, Nguyen LS, Nicouleau M, Lipecka J, Bizot J-C, Thiel C, Foulquier F, Lefort N, Faivre-Sarrailh C *et al* (2018) High N-glycan multiplicity is critical for neuronal adhesion and sensitizes the developing cerebellum to N-glycosylation defect. *Elife* 7: e38309

Metzler M, Gertz A, Sarkar M, Schachter H, Schrader JW, Marth JD (1994) Complex asparagine-linked oligosaccharides are required for morphogenic events during post-implantation development. *EMBO J* 13: 2056 – 2065

Minevich G, Park DS, Blankenberg D, Poole RJ, Hobert O (2012) CloudMap: a cloud-based pipeline for analysis of mutant genome sequences. *Genetics* 192: 1249 – 1269

Mire E, Hocine M, Bazellieres E, Jungas T, Davy A, Chauvet S, Mann F (2018) Developmental upregulation of Ephrin-B1 silences Sema3C/Neuropilin-1 signaling during post-crossing navigation of corpus callosum axons. *Curr Biol* 28: 1768 – 1782

Moloney DJ, Panin VM, Johnston SH, Chen J, Shao LI, Wilson R, Wang Y, Stanley P, Irvine KD, Haltiwanger RS *et al* (2000) Fringe is a glycosyltransferase that modifies Notch. *Nature* 406: 369 – 375

Moremen KW (2002) Golgi α-mannosidase II deficiency in vertebrate systems: implications for asparagine-linked oligosaccharide processing in mammals. *Biochem Biophys Acta* 1573: 225 – 235

Ng BG, Freeze HH (2018) Perspectives on glycosylation and its congenital disorders. *Trends Genet* 34: 466 – 476

Okkema PG, Harrison SW, Plunger V, Aryana A, Fire A (1993) Sequence requirements for myosin gene expression and regulation in *Caenorhabditis elegans*. *Genetics* 135: 385 – 404

Oren-Suissa M, Hall DH, Treinin M, Shemer G, Podbilewicz B (2010) The fusogen EFF-1 controls sculpting of mechanosensory dendrites. *Science* 328: 1285 – 1288

Paschinger K, Hackl M, Gutternigg M, Kretschmer-Lubich D, Stemmer U, Jantsch V, Lochnit G, Wilson IB (2006) A deletion in the golgi alpha-mannosidase II gene of *Caenorhabditis elegans* results in unexpected non-wild-type N-glycan structures. *J Biol Chem* 281: 28265 – 28277

Paschinger K, Yan S, Wilson IBH (2019) N-glycomic complexity in anatomical simplicity: *Caenorhabditis elegans* as a non-model nematode? *Front Mol Biosci* 6: 9

Poulain FE, Yost HJ (2015) Heparan sulfate proteoglycans: a sugar code for vertebrate development? *Development* 142: 3456 – 3467

Riley NM, Hebert AS, Westphall MS, Coon JJ (2019) Capturing site-specific heterogeneity with large-scale N-glycoproteome analysis. *Nat Commun* 10: 1311

Saied-Santiago K, Bülow HE (2018) Diverse roles for glycosaminoglycans in neural patterning. *Dev Dyn* 247: 54 – 74

Salzberg Y, Coleman AJ, Celestrin K, Cohen-Berkman M, Biederer T, Henis-Korenblit S, Bülow HE (2017) Reduced Insulin/Insulin-like growth factor receptor signaling mitigates defective dendrite morphogenesis in mutants of the ER stress sensor IRE-1. *PLoS Genet* 13: e1006579

Salzberg Y, Diaz-Balzac CA, Ramirez-Suarez NJ, Attreed M, Tecle E, Desbois M, Kaprielian Z, Bülow HE (2013) Skin-derived cues control arborization of sensory dendrites in *Caenorhabditis elegans*. *Cell* 155: 308 – 320

Salzberg Y, Ramirez-Suarez NJ, Bülow HE (2014) The proprotein convertase KPC-1/furin controls branching and self-avoidance of sensory dendrites in Caenorhabditis elegans. *PLoS Genet* 10: e1004657

Schnaar RL, Gerardy-Schahn R, Hildebrandt H (2014) Sialic acids in the brain: gangliosides and polysialic acid in nervous system development, stability, disease, and regeneration. *Physiol Rev* 94: 461 – 518

Schroeder NE, Androwski RJ, Rashid A, Lee H, Lee J, Barr MM (2013) Dauer-specific dendrite arborization in *C. elegans* is regulated by KPC-1/Furin. *Curr Biol* 23: 1527 – 1535

Sekine SU, Haraguchi S, Chao K, Kato T, Luo L, Miura M, Chihara T (2013) Meigo governs dendrite targeting specificity by modulating ephrin level and N-glycosylation. *Nat Neurosci* 16: 683 – 691

Shah N, Kuntz DA, Rose DR (2008) Golgi alpha-mannosidase II cleaves two sugars sequentially in the same catalytic site. *Proc Natl Acad Sci USA* 105: 9570 – 9575

Smith C, O'Brien T, Chatzigeorgiou M, Spencer W, Feingold-Link E, Husson S, Hori S, Mitani S, Gottschalk A, Schafer W *et al* (2013) Sensory neuron fates are distinguished by a transcriptional switch that regulates dendrite branch stabilization. *Neuron* 79: 266 – 280

Smith CJ, Watson JD, Spencer WC, O'Brien T, Cha B, Albeg A, Treinin M, Miller III DM (2010) Time-lapse imaging and cell-specific expression profiling reveal dynamic branching and molecular determinants of a multi-dendritic nociceptor in C. elegans. *Dev Biol* 345: 18 – 33

Stanley P, Taniguchi N, Aebi M (2015) N-Glycans, In *Essentials of Glycobiology*, Stanley P, Taniguchi N, Aebi M, Varki A, Cummings RD, Esko JD, Stanley P, Hart GW, Aebi M, Darvill AG, Kinoshita T, Packer NH *et al* (eds), pp 99 – 111. New York, NY: Cold Spring Harbor

Sundararajan L, Stern J, Miller 3rd DM (2019) Mechanisms that regulate morphogenesis of a highly branched neuron in *C. elegans*. *Dev Biol* 451: 53 – 67

Tang LT, Diaz-Balzac CA, Rahman M, Ramirez-Suarez NJ, Salzberg Y, Lazaro-Pena MI, Bülow HE (2019) TIAM-1/GEF can shape somatosensory dendrites independently of its GEF activity by regulating F-actin localization. *Elife* 8: e38949

Tao L, Porto D, Li Z, Fechner S, Lee SA, Goodman MB, Xu XZS, Lu H, Shen K (2019) Parallel processing of two mechanosensory modalities by a single neuron in *C. elegans*. *Dev Cell* 51: 617 – 631.e3

Taylor SR, Santpere G, Weinreb A, Barrett A, Reilly MB, Xu C, Varol E, Oikonomou P, Glenwinkel L, McWhirter R *et al* (2021) Molecular topography of an entire nervous system. *Cell* 184: 4329 – 4347

Thompson O, Edgley M, Strasbourger P, Flibotte S, Ewing B, Adair R, Au V, Chaudhry I, Fernando L, Hutter H *et al* (2013) The million mutation project: a new approach to genetics in *Caenorhabditis elegans*. *Genome Res* 23: 1749 – 1762

Tsalik EL, Niacaris T, Wenick AS, Pau K, Avery L, Hobert O (2003) LIM homeobox gene-dependent expression of biogenic amine receptors in restricted regions of the *C. elegans* nervous system. *Dev Biol* 263: 81 – 102

Vabulas RM, Raychaudhuri S, Hayer-Hartl M, Hartl FU (2010) Protein folding in the cytoplasm and the heat shock response. *Cold Spring Harb Perspect Biol* 2: a004390

Wei X, Howell AS, Dong X, Taylor CA, Cooper RC, Zhang J, Zou W, Sherwood DR, Shen K (2015) The unfolded protein response is required for dendrite morphogenesis. *Elife* 4: e06963

Zou W, Shen A, Dong X, Tugizova M, Xiang YK, Shen K (2016) A multi-protein receptor-ligand complex underlies combinatorial dendrite guidance choices in *C. elegans*. *Elife* 5: e18345

